

Fundamental limits on the rate of bacterial cell division

Nathan M. Belliveau^{†, 1}, Griffin Chure^{†, 2, 3}, Christina L. Hueschen⁴, Hernan G. Garcia⁵, Jané Kondev⁶, Daniel S. Fisher⁷, Julie Theriot^{1, 8}, Rob Phillips^{2, 9, *}

*For correspondence:

[†]These authors contributed equally to this work

¹Department of Biology, University of Washington, Seattle, WA, USA; ²Division of Biology and Biological Engineering, California Institute of Technology, Pasadena, CA, USA; ³Department of Applied Physics, California Institute of Technology, Pasadena, CA, USA; ⁴Department of Chemical Engineering, Stanford University, Stanford, CA, USA; ⁵Department of Molecular Cell Biology and Department of Physics, University of California Berkeley, Berkeley, CA, USA; ⁶Department of Physics, Brandeis University, Waltham, MA, USA; ⁷Department of Applied Physics, Stanford University, Stanford, CA, USA; ⁸Allen Institute for Cell Science, Seattle, WA, USA; ⁹Department of Physics, California Institute of Technology, Pasadena, CA, USA; *Contributed equally

Abstract

Introduction

The range of bacterial growth rates is enormously diverse. In natural environments, some microbial organisms might double only once per year while in comfortable laboratory conditions, growth can be rapid with several divisions per hour. This six order of magnitude difference illustrates the intimate relationship between environmental conditions and the rates at which cells convert nutrients into new cellular material – a relationship that has remained a major topic of inquiry in bacterial physiology for over a century (28). As was noted by Jacques Monod, “the study of the growth of bacterial cultures does not constitute a specialized subject or branch of research, it is the basic method of Microbiology.” Those words ring as true today as they did when they were written 70 years ago. Indeed, the study of bacterial growth has undergone a molecular resurgence since many of the key questions addressed by the pioneering efforts in the middle of the last century can be revisited by examining them through the lens of the increasingly refined molecular census that is available for bacteria such as the microbial workhorse *Escherichia coli*. Several of the outstanding questions that can now be studied about bacterial growth include: what sets the fastest time scale that bacteria can divide, and how is growth rate tied to the quality of the carbon source. In this paper, we address these two questions from two distinct angles. First, as a result of an array of high-quality proteome-wide measurements of the *E. coli* proteome under a myriad of different growth conditions, we have a census that allows us to explore how the number of key molecular players change as a function of growth rate. This census provides a window onto whether the processes they mediate such as molecular transport into the cells and molecular synthesis within cells can run faster. Second, because of our understanding of the molecular pathways responsible for many of the steps in bacterial growth, we can also make order of magnitude estimates to infer the copy numbers that would be needed to achieve a given growth rate. In this paper, we pass back and forth between the analysis of a variety of different proteomic datasets and order-of-magnitude estimations to determine possible molecular bottlenecks that limit bacterial growth and to see how

42 the growth rate varies in different carbon sources.

43 Specifically, we leverage a combination of *E. coli* proteomic data sets collected over the past
 44 decade using either mass spectrometry (48; 40; 61) or ribosomal profiling (31) across 31 unique
 45 growth conditions. Broadly speaking, we entertain several classes of hypotheses as are illustrated
 46 in **Figure 1**. First, we consider potential limits on the transport of nutrients into the cell. We address
 47 this hypothesis by performing an order-of-magnitude estimate for how many carbon, phosphorous,
 48 and sulfur atoms are needed to facilitate this requirement given a 5000 second division time. As a
 49 second hypothesis, we consider the possibility that there exists a fundamental limit on how quickly
 50 the cell can generate ATP. We approach this hypothesis from two angles, considering how many
 51 ATP synthase complexes must be needed to churn out enough ATP to power protein translation
 52 followed by an estimation of how many electron transport complexes must be present to maintain
 53 the proton motive force. A third class of estimates considers the need to maintain the size and
 54 shape of the cell through the construction of new lipids for the cell membranes as well as the glycan
 55 polymers which make up the rigid peptidoglycan. Our final class of hypotheses centers on the
 56 synthesis of a variety of biomolecules. Our focus is primarily on the stages of the central dogma
 57 as we estimate the number of protein complexes needed for DNA replication, transcription, and
 58 protein translation.

59 In broad terms, we find that the majority of these estimates are in close agreement with the
 60 experimental observations, with protein copy numbers apparently well-tuned for the task of cell
 61 doubling. This allows us to systematically scratch off the hypotheses diagrammed in **Figure 1** as
 62 setting possible speed limits. Ultimately, we find that protein translation (particularly the generation
 63 of new ribosomes) acts as 1) a rate limiting step for the *fastest* bacterial division, and 2) the major
 64 determinant of bacterial growth across all nutrient conditions we have considered under steady
 65 state, exponential growth. This perspective is in line with the linear correlation observed between
 66 growth rate and ribosomal content (typically quantified through the ratio of RNA to protein) for fast
 67 growing cells (50), but suggests a more prominent role for ribosomes in setting the doubling time
 68 across all conditions of nutrient limitation. Here we again leverage the quantitative nature of this
 69 data set and present a quantitative model of the relationship between the fraction of the proteome
 70 devoted to ribosomes and the speed limit of translation, revealing a fundamental tradeoff between
 71 the translation capacity of the ribosome pool and the maximal growth rate.

72 Uptake of Nutrients

73 In order to build new cellular mass, the molecular and elemental building blocks must be scavenged
 74 from the environment in different forms. Carbon, for example, is acquired via the transport of
 75 carbohydrates and sugar alcohols with some carbon sources receiving preferential treatment in their
 76 consumption (35). Phosphorus, sulfur, and nitrogen, on the other hand, are harvested primarily in
 77 the forms of inorganic salts, namely phosphate, sulfate, and ammonia (28; 6; 55; 4; 44; 63). All of
 78 these compounds have different permeabilities across the cell membrane and most require some
 79 energetic investment either via ATP hydrolysis or through the proton electrochemical gradient to
 80 bring the material across the hydrophobic cell membrane. Given the diversity of biological transport
 81 mechanisms and the vast number of inputs needed to build a cell, we begin by considering transport
 82 of some of the most important cellular ingredients: carbon, nitrogen, oxygen, hydrogen, phosphorus,
 83 and sulfur.

84 The elemental composition of *E. coli* has received much quantitative attention over the past half
 85 century (38; 60; 23; 7), providing us with a starting point for estimating the copy numbers of various
 86 transporters. While there is some variability in the exact elemental percentages (with different
 87 uncertainties), we can estimate that the dry mass of a typical *E. coli* cell is \approx 45% carbon (BNID:
 88 100649, (34)), \approx 15% nitrogen (BNID: 106666, (34)), \approx 3% phosphorus (BNID: 100653, (34)), and
 89 1% sulfur (BNID: 100655, (34)). In the coming paragraphs, we will engage in a dialogue between
 90 back-of-the-envelope estimates for the numbers of transporters needed to facilitate these chemical
 91 stoichiometries and the experimental proteomic measurements of the biological reality. Such an

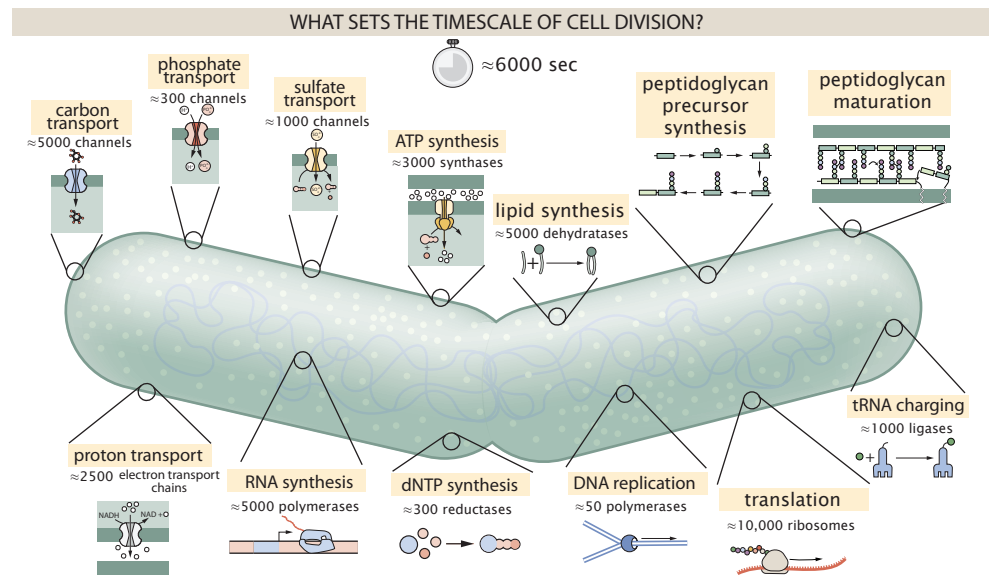


Figure 1. Transport and synthesis processes necessary for cell division. We consider an array of processes necessary for a cell to double its molecular components. Such processes include the transport of carbon across the cell membrane, the production of ATP, and fundamental processes of the central dogma namely RNA, DNA, and protein synthesis. A schematic of each synthetic or transport category is shown with an approximate measure of the complex abundance at a growth rate of 0.5 per hour. In this work, we consider a standard bacterial division time of ≈ 5000 sec.

92 approach provides the opportunity to test if our biological knowledge is sufficient to understand the
 93 scale at which these complexes are produced. Specifically, we will make these estimates considering
 94 a modest doubling time of 5000 s, a growth rate of $\approx 0.5 \text{ hr}^{-1}$, the range in which the majority of the
 95 experimental measurements reside.

96 Carbon Transport

97 We begin with the most abundant element by mass, carbon. Using $\approx 0.3 \text{ pg}$ as the typical *E. coli*
 98 dry mass (BNID: 103904, (34)), we estimate that $\approx 10^{10}$ carbon atoms must be brought into the
 99 cell in order to double all of the carbon-containing molecules (**Figure 2(A, top)**). Typical laboratory
 100 growth conditions, such as those explored in the aforementioned proteomic data sets, provide
 101 carbon as a single class of sugar such as glucose, galactose, or xylose to name a few. *E. coli* has
 102 evolved myriad mechanisms by which these sugars can be transported across the cell membrane.
 103 One such mechanism of transport is via the PTS system which is a highly modular system capable
 104 of transporting a diverse range of sugars (14). The glucose-specific component of this system
 105 transports ≈ 200 glucose molecules per second per channel (BNID: 114686, (34)). Making the
 106 assumption that this is a typical sugar transport rate, coupled with the need to transport 10^{10} carbon
 107 atoms, we arrive at the conclusion that on the order of 1,000 transporters must be expressed
 108 in order to bring in enough carbon atoms to divide in 6,000 s, diagrammed in the top panel of
 109 **Figure 2(A)**. This estimate, along with the observed average number of carbohydrate transporters
 110 present in the proteomic data sets (48; 40; 61; 31), is shown in **Figure 2(A)**. While we estimate 1,000
 111 transporters are needed, the data reveals that at a division time of ≈ 5000 s there is nearly a ten-fold
 112 excess of transporters. Furthermore, the data illustrates that the average number of carbohydrate
 113 transporters present is largely-growth rate independent.

114 The estimate presented in **Figure 2(A)** neglects any specifics of the regulation of carbon transport
 115 system and presents a data-averaged view of how many carbohydrate transporters are present
 116 on average. Using the diverse array of growth conditions explored in the proteomic data sets, we
 117 can explore how individual carbon transport systems depend on the population growth rate. In

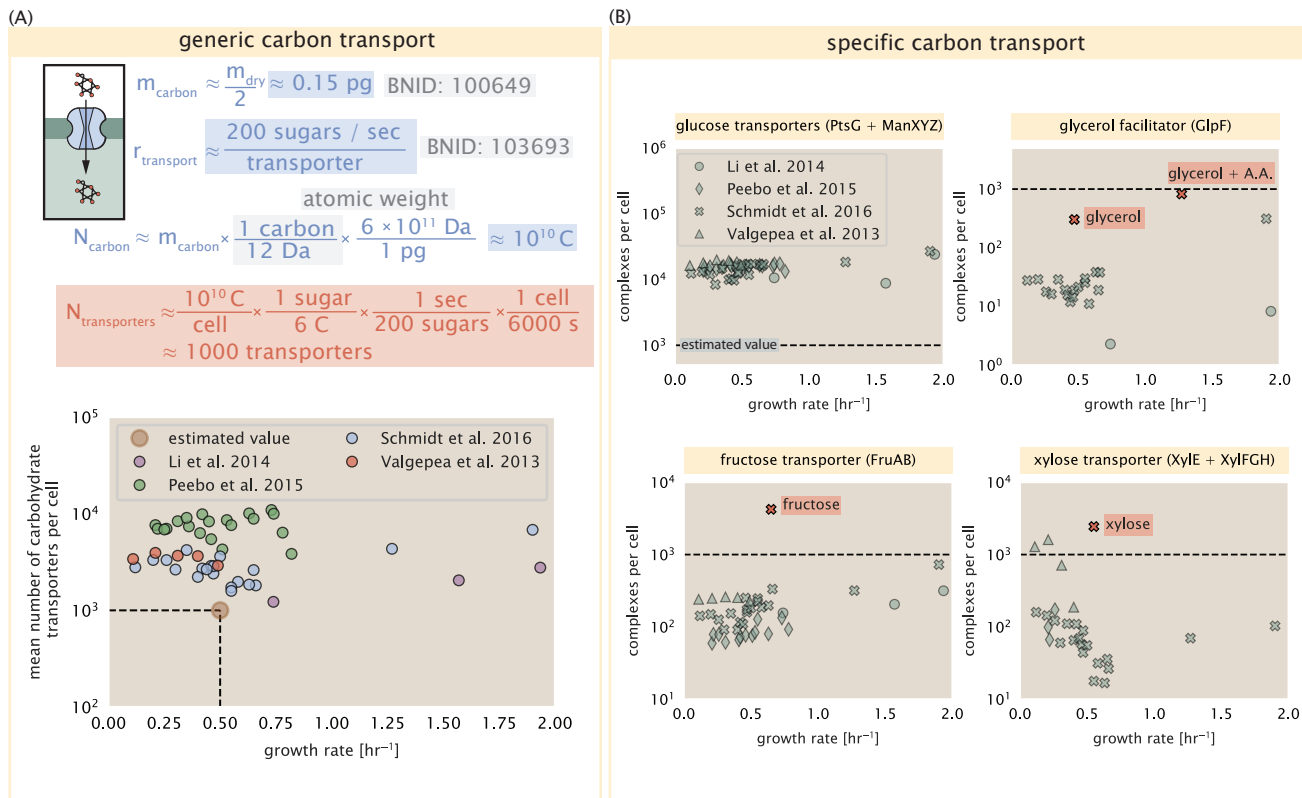


Figure 2. The abundance of carbon transport systems across growth rates. (A) A simple estimate for the minimum number of generic carbohydrate transport systems (top) assumes $\approx 10^{10}$ C are needed to complete division, each transported sugar contains ≈ 6 C, and each transporter conducts sugar molecules at a rate of ≈ 200 per second. Bottom plot shows the estimated number of transporters needed at a growth rate of ≈ 0.5 per hr (light-brown point and dashed lines). Colored points correspond to the mean number of carbohydrate transporters for different growth conditions across different published datasets. (B) The abundance of various specific carbon transport systems plotted as a function of the population growth rate. Red points and red-highlighted text indicate conditions in which the only source of carbon in the growth medium induces expression of the transport system.

118 **Figure 2(B)**, we show the total number of carbohydrate transporters specific to different carbon
 119 sources. A striking observation, shown in the top-left plot of **Figure 2(B)**, is the constancy in the
 120 expression of the glucose-specific transport systems (the PtsG enzyme of the PTS system and the
 121 glucose-transporting ManXYZ complex). Additionally, we note that the total number of glucose-
 122 specific transporters is tightly distributed $\approx 10^4$ per cell, an order of magnitude beyond the estimate
 123 shown in **Figure 2(A)**. This illustrates that *E. coli* maintains a substantial number of complexes
 124 present for transporting glucose which is known to be the preferential carbon source (35; 33; 3).

125 It is now understood that a large number of metabolic operons are regulated with dual-input
 126 logic gates that are only expressed when glucose concentrations are low (mediated by cyclic-AMP
 127 receptor protein CRP) and the concentration of other carbon sources are elevated (19; 65). A famed
 128 example of such dual-input regulatory logic is in the regulation of the *lac* operon which is only
 129 natively activated in the absence of glucose and the presence of allolactose, an intermediate in
 130 lactose metabolism (26), though we now know of many other such examples (25; 19; 8). This
 131 illustrates that once glucose is depleted from the environment, cells have a means to dramatically
 132 increase the abundance of the specific transporter needed to digest the next sugar that is present.
 133 Several examples of induced expression of specific carbon-source transporters are shown in
 134 **Figure 2(B)**. Points colored in red (labeled by red text-boxes) correspond to growth conditions in
 135 which the specific carbon source (glycerol, xylose, or fructose) is present. These plots show that, in
 136 the absence of the particular carbon source, expression of the transporters is maintained on the
 137 order of $\sim 10^2$ per cell. However, when induced, the transporters become highly-expressed and
 138 are present on the order of $\sim 10^4$ per cell, which exceeds the generic estimation given in **Figure 2(A)**.
 139 Together, this generic estimation and the specific examples of induced expression suggest that
 140 transport of carbon across the cell membrane, while critical for growth, is not the rate-limiting step
 141 of cell division.

142 In the context of speeding up growth, one additional limitation is the fact that the cell's inner
 143 membrane is occupied by a multitude of other membrane proteins. Considering a rule-of-thumb
 144 for the surface area of *E. coli* of about $6 \mu\text{m}^2$ (BNID: 101792, (34)), we expect an areal density for
 145 1,000 transporters to be approximately 200 transporters/ μm^2 . For a glucose transporter occupying
 146 about $50 \text{ nm}^2/\text{dimer}$, this amounts to about only 1 percent of the total inner membrane (58). In
 147 addition, bacterial cell membranes typically have densities of 10^5 proteins// μm^2 (42), implying that
 148 the cell could accommodate more transporters if it were rate limiting.

149 Phosphorus and Sulfur Transport

150 We now turn our attention towards other essential elements, namely phosphorus and sulfur.
 151 Phosphorus is critical to the cellular energy economy in the form of high-energy phosphodiester
 152 bonds making up DNA, RNA, and the NTP energy pool as well as playing a critical role in the post-
 153 translational modification of proteins and defining the polar-heads of lipids. In total, phosphorus
 154 makes up $\approx 3\%$ of the cellular dry mass which in typical experimental conditions is in the form of
 155 inorganic phosphate. The cell membrane has remarkably low permeability to this highly-charged
 156 and critical molecule, therefore requiring the expression of active transport systems. In *E. coli*, the
 157 proton electrochemical gradient across the inner membrane is leveraged to transport inorganic
 158 phosphate into the cell (44). Proton-solute symporters are widespread in *E. coli* (43; 10) and can
 159 have rapid transport rates of 50 molecules per second for sugars and other solutes (BNID: 103159;
 160 111777, (34)). In *E. coli* the PitA phosphate transport system has been shown to very tightly coupled
 161 with the proton electrochemical gradient with a 1:1 proton:phosphate stoichiometric ratio (22; 15).
 162 Illustrated in **Figure 3(A)**, we can estimate that ≈ 300 phosphate transporters are necessary to
 163 maintain an $\approx 3\%$ dry mass with a 6,000 s division time. This estimate is again satisfied when we
 164 examine the observed copy numbers of PitA in proteomic data sets (plot in **Figure 3(A)**). While our
 165 estimate is very much in line with the observed numbers, we emphasize that this is likely a slight
 166 over estimate of the number of transporters needed as there are other phosphorous scavenging
 167 systems, such as the ATP-dependent phosphate transporter Pst system which we have neglected.

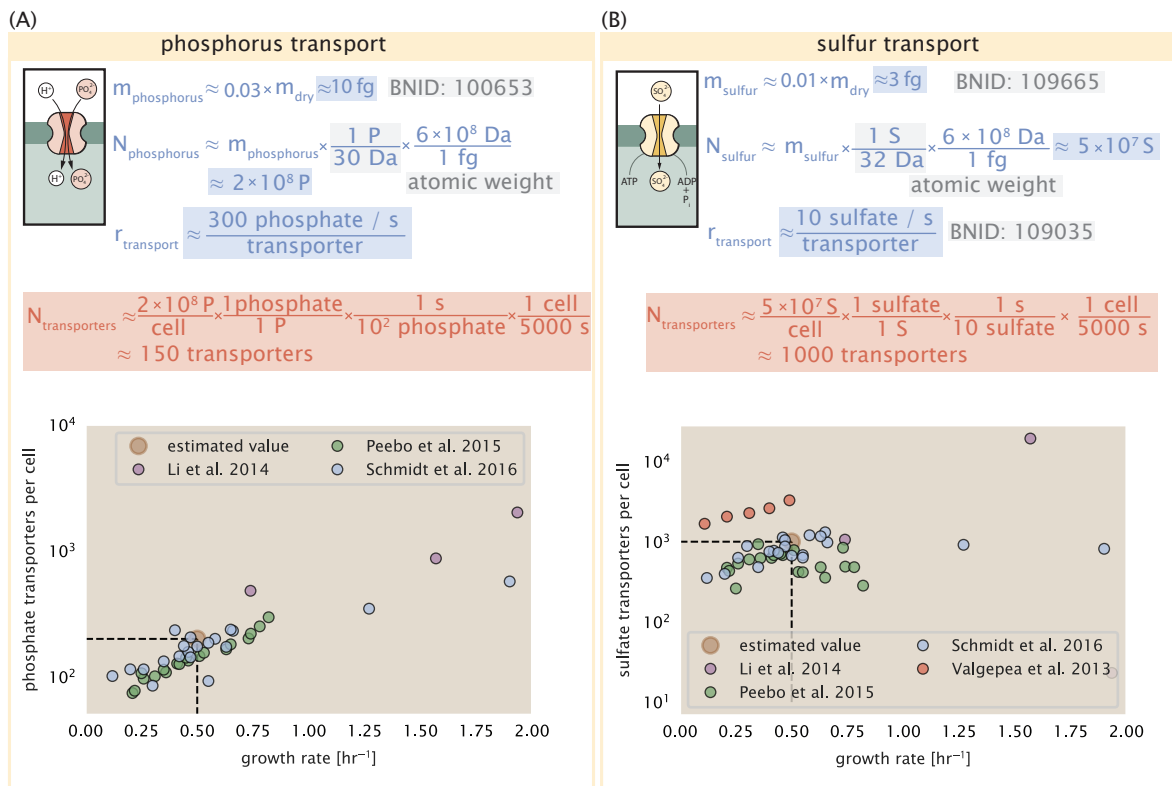


Figure 3. Estimates and measurements of phosphate and sulfate transport systems as a function of growth rate. (A) Estimate for the number of PitA phosphate transport systems needed to maintain a 3% phosphorus *E. coli* dry mass. Points in plot correspond to the total number of PitA transporters per cell. (B) Estimate of the number of CysUWA complexes necessary to maintain a 1% sulfur *E. coli* dry mass. Points in plot correspond to average number of CysUWA transporter complexes that can be formed given the transporter stoichiometry [CysA]₂[CysU][CysW][Sbp/CysP].

168 Satisfied that there are a sufficient number of phosphate transporters present in the cell, we now
 169 turn to sulfur transport as another potentially rate limiting process. Similar to phosphate, sulfate is
 170 highly-charged and not particularly membrane permeable, requiring active transport. While there
 171 exists a H⁺/sulfate symporter in *E. coli*, it is in relatively low abundance and is not well characterized
 172 (64). Sulfate is predominantly acquired via the ATP-dependent ABC transporter CysUWA system
 173 which also plays an important role in selenium transport (51; 54). While specific kinetic details
 174 of this transport system are not readily available, generic ATP transport systems in prokaryotes
 175 transport on the order of 1 to 10 molecules per second (BNID: 109035, (34)). Combining this generic
 176 transport rate, measurement of sulfur comprising 1% of dry mass, and a 6,000 second division time
 177 yields an estimate of ≈ 1000 CysUWA complexes per cell (*Figure 3(B)*). Once again, this estimate is
 178 in notable agreement with proteomic data sets, suggesting that there are sufficient transporters
 179 present to acquire the necessary sulfur. In a similar spirit of our estimate of phosphorus transport,
 180 we emphasize that this is likely an overestimate of the number of necessary transporters as we
 181 have neglected other sulfur scavenging systems that are in lower abundance.

182 Nitrogen Transport

183 Finally, we turn to nitrogen transport as the last remaining transport system highlighted in *Figure 1*.
 184 Unlike phosphate, sulfate, and various sugar molecules, nitrogen in the form of ammonia can
 185 readily diffuse across the cell membrane and has a permeability on par with water ($\approx 10^5$ nm/s,
 186 BNID:110824 (34)). In particularly nitrogen-poor conditions, *E. coli* expresses a transporter (AmtB)
 187 which appears to aid in nitrogen assimilation, though the mechanism and kinetic details of transport
 188 is still a matter of debate (62; 30). Beyond ammonia, another plentiful source of nitrogen come in

189 the form of glutamate, which has its own complex metabolism and scavenging pathways. However,
 190 nitrogen is plentiful in the growth conditions examined in this work, permitting us to neglect
 191 nitrogen transport as a potential rate limiting process in cell division.

192 Function of the Central Dogma

193 Up to this point, we have considered a variety of transport and biosynthetic processes that are
 194 critical to acquiring and generating new cell mass. While there are of course many other metabolic
 195 processes we could consider and perform estimates of (such as the components of fermentative
 196 versus aerobic respiration), we now turn our focus to some of the most central processes which
 197 must be undertaken irrespective of the growth conditions – the processes of the central dogma.

198 DNA

199 Most bacteria (including *E. coli*) harbor a single, circular chromosome and can have extra-chromosomal
 200 plasmids up to ~ 100 kbp in length. We will focus our quantitative thinking solely on the chromo-
 201 some of *E. coli* which harbors ≈ 5000 genes and ≈ 5 × 10⁶ base pairs. To successfully divide and
 202 produce viable progeny, this chromosome must be faithfully replicated and segregated into each
 203 nascent cell. We again rely on the near century of literature in molecular biology to provide some
 204 insight on the rates and mechanics of the replicative feat as well as the production of the required
 205 starting materials, dNTPs.

206 dNTP synthesis

207 We begin our exploration DNA replication by examining the production of the deoxyribonucleotide
 208 triphosphates (dNTPs). The four major dNTPs (dATP, dTTP, dCTP, and dGTP) are synthesized *de novo*
 209 in separate pathways, requiring different building blocks. However, a critical step present in all dNTP
 210 synthesis pathways is the conversion from ribonucleotide to deoxyribonucleotide via the removal
 211 of the 3' hydroxyl group of the ribose ring (45). This reaction is mediated by a class of enzymes
 212 termed ribonucleotide reductases, of which *E. coli* possesses two aerobically active complexes
 213 (termed I and II) and a single anaerobically active enzyme. Due to their peculiar formation of
 214 a radical intermediate, these enzymes have received much biochemical, kinetic, and structural
 215 characterization. One such work (20) performed a detailed *in vitro* measurement of the steady-state
 216 kinetic rates of these complexes, revealing a turnover rate of ≈ 10 dNTP per second.

217 Since this reaction is central to the synthesis of all dNTPs, it is reasonable to consider the
 218 abundance of these complexes is a measure of the total dNTP production in *E. coli*. Illustrated
 219 schematically in **Figure 4** (A), we consider the fact that to replicate the cell's genome, on the order of
 220 ≈ 10⁷ dNTPs must be synthesized. Assuming a production rate of 10 per second per ribonucleotide
 221 reductase complex and a cell division time of 6000 seconds, we arrive at an estimate of ≈ 150
 222 complexes needed per cell. As shown in the bottom panel of **Figure 4** (A), this estimate agrees
 223 with the experimental measurements of these complexes abundances within ≈ 1/2 an order of
 224 magnitude.

225 Recent work has revealed that during replication, the ribonucleotide reductase complexes
 226 coalesce to form discrete foci colocalized with the DNA replisome complex (46). This is particularly
 227 pronounced in conditions where growth is slow, indicating that spatial organization and regulation
 228 of the activity of the complexes plays an important role.

229 DNA Replication

230 We now turn our focus to the integration of these dNTP building blocks into the replicated chromo-
 231 some strand via the DNA polymerase. Replication is initiated at a single region of the chromosome
 232 termed the *oriC* locus at which a pair of DNA polymerases bind and begin their high-fidelity replica-
 233 tion of the genome in opposite directions. Assuming equivalence between the two replication forks,
 234 this means that the two DNA polymerase complexes (termed replisomes) meet at the midway point
 235 of the circular chromosome termed the *ter* locus. The kinetics of the five types of DNA polymerases

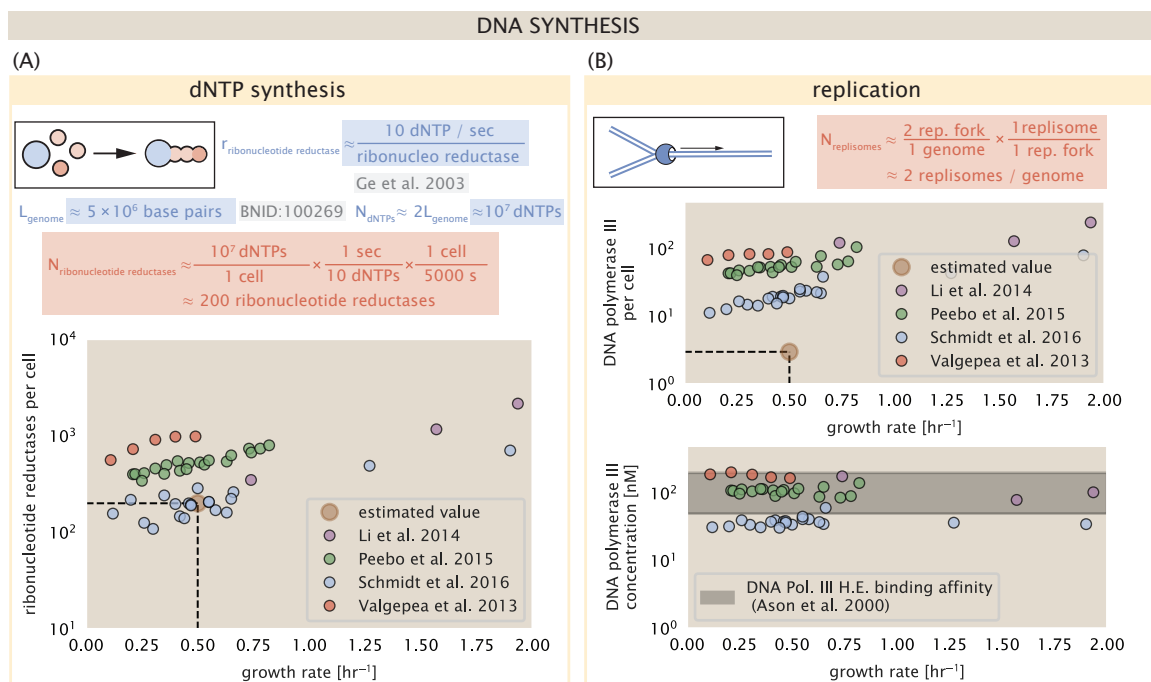


Figure 4. Complex abundance estimates for dNTP synthesis and DNA replication. (A) Estimate of the number of ribonucleotide reductase enzymes needed to facilitate the synthesis of $\approx 10^7$ dNTPs over the course of a 6000 second generation time. Points in the plot correspond to the total number of ribonucleotide reductase I ($[NrdA]_2[NrdB]_2$) and ribonucleotide reductase II ($[NrdE]_2[NrdF]_2$) complexes. (B) An estimate for the minimum number of DNA polymerase holoenzyme complexes needed to facilitate replication of a single genome. Points in the top plot correspond to the total number of DNA polymerase III holoenzyme complexes ($[DnaE]_3[DnaQ]_3[HolE]_3[DnaX]_5[HolB][HolA][DnaN]_4[HolC]_4[HolD]_4$) per cell. Bottom plot shows the effective concentration of DNA polymerase III holoenzyme given cell volumes calculated from the growth rate as in (52) (See Appendix Section 4).

(I – V) have been intensely studied, revealing that DNA polymerase III performs the high fidelity processive replication of the genome with the other "accessory" polymerases playing auxiliary roles (17). *In vitro* measurements have shown that DNA Polymerase III copies DNA at a rate of \approx 600 nucleotides per second (BNID: 104120, (34)). Therefore, to replicate a single chromosome, two DNA polymerases replicating at their maximal rate would copy their entire genome in \approx 4000 s. Thus, with a division time of 5000 s (our "typical" growth rate for the purposes of this work), there is sufficient time for a pair of DNA polymerase III complexes to replicate the entire genome. However, this estimate implies that 4000 s would be the upper-limit time scale for bacterial division which is at odds with the familiar 20 minute (1200 s) doubling time of *E. coli* in rich medium.

It is well known that *E. coli* can parallelize its DNA replication such that multiple chromosomes are being replicated at once, with as many as 10 - 12 replication forks at a given time (11; 53). Thus, even in rapidly growing cultures, we expect only a few polymerases (\approx 10) are needed to replicate the chromosome per cell doubling. However, as shown in **Figure 4(B)**, DNA polymerase III is nearly an order of magnitude more abundant. This discrepancy can be understood by considering its binding constant to DNA. DNA polymerase III is highly processive, facilitated by a strong affinity of the complex to the DNA. *In vitro* biochemical characterization has quantified the K_D of DNA polymerase III holoenzyme to single-stranded and double-stranded DNA to be 50 and 200 nM, respectively (5). The bottom plot in **Figure 4 (B)** shows that the concentration of the DNA polymerase III across all data sets and growth conditions is within this range. Thus, while the copy number of the DNA polymerase III is in excess of the strict number required to replicate the genome, its copy number appears to vary such that its concentration is approximately equal to the dissociation constant to the DNA. While the processes regulating the initiation of DNA replication are complex and involve more than just the holoenzyme, these data indicate that the kinetics of replication rather than the explicit copy number of the DNA polymerase III holoenzyme is the more relevant feature of DNA replication to consider. In light of this, the data in **Figure 4(B)** suggests that for bacteria like *E. coli*, DNA replication does not represent a rate-limiting step in cell division. However, it is worth noting that for bacterium like *C. crescentus* whose chromosomal replication is initiated only once per cell cycle (27), the time to double their chromosome likely represents an upper limit to their growth rate.

265 RNA Synthesis

With the machinery governing the replication of the genome accounted for, we now turn our attention to the next stage of the central dogma – the transcription of DNA to form RNA. We primarily consider three major groupings of RNA, namely the RNA associated with ribosomes (rRNA), the RNA encoding the amino-acid sequence of proteins (mRNA), and the RNA which links codon sequence to amino-acid identity during translation (tRNA). Despite the varied function of these RNA species, they share a commonality in that they are transcribed from DNA via the action of RNA polymerase. In the coming paragraphs, we will consider the synthesis of RNA as a rate limiting step in bacterial division by estimating how many RNA polymerases must be present to synthesize all necessary rRNA, mRNA, and tRNA.

275 rRNA

We begin with an estimation of the number of RNA polymerases needed to synthesize the rRNA that serve as catalytic and structural elements of the ribosome. Each ribosome contains three rRNA molecules of lengths 120, 1542, and 2904 nucleotides (BNID: 108093, (34)), meaning each ribosome contains \approx 4500 nucleotides. As the *E. coli* RNA polymerase transcribes DNA to RNA at a rate of \approx 40 nucleotides per second (BNID: 101904, (34)), it takes a single RNA polymerase \approx 100 s to synthesize the RNA needed to form a single functional ribosome. Therefore, in a 5000 s division time, a single RNA polymerase transcribing rRNA at a time would result in only \approx 50 functional ribosomal rRNA units – far below the observed number of \approx 10^4 ribosomes per cell.

284 Of course, there can be more than one RNA polymerase transcribing the rRNA genes at any

given time. To elucidate the *maximum* number of rRNA units that can be synthesized given a single copy of each rRNA gene, we will consider a hypothesis in which the rRNA operon is completely tiled with RNA polymerase. *In vivo* measurements of the kinetics of rRNA transcription have revealed that RNA polymerases are loaded onto the promoter of an rRNA gene at a rate of ≈ 1 per second (BNID: 111997; 102362, (34)). If RNA polymerases are being constantly loaded on to the rRNA genes at this rate, then we can assume that ≈ 1 functional rRNA unit is synthesized per second. With a 5000 second division time, this hypothesis leads to a maximal value of 5000 functional rRNA units, still undershooting the observed number of 10^4 ribosomes per cell.

E. coli has evolved a clever mechanism to surpass this kinetic limit for the rate of rRNA production. Rather than having only one copy of each rRNA gene, *E. coli* has seven copies of the operon (BIND: 100352, (34)) four of which are localized directly adjacent to the origin of replication (9). As fast growth also implies an increased gene dosage due to parallelized chromosomal replication, the total number of rRNA genes can be on the order of $\approx 10 - 70$ copies at moderate to fast growth rates (56). Using our standard time scale of a 5000 second division time, we can make the lower-bound estimate that the typical cell will have 7 copies of the rRNA operon. Synthesizing one functional rRNA unit per second per rRNA operon, a total of 4×10^4 rRNA units can be synthesized, comfortably above the observed number of ribosomes per cell.

How many RNA polymerases are then needed to constantly transcribe 7 copies of the rRNA genes? We approach this estimate by considering the maximum number of RNA polymerases tiled along the rRNA genes with a loading rate of 1 per second and a transcription rate of 40 nucleotides per second. Considering that a RNA polymerase has a physical footprint of approximately 40 nucleotides (BNID: 107873, (34)), we can expect ≈ 1 RNA polymerase per 80 nucleotides. With a total length of ≈ 4500 nucleotides per operon and 7 operons per cell, the maximum number of RNA polymerases that can be transcribing rRNA at any given time is ≈ 400 . As we will see in the coming sections, the synthesis of rRNA is the dominant requirement of the RNA polymerase pool.

310 mRNA

311 To form a functional protein, all protein coding genes must first be transcribed from DNA to form
 312 an mRNA molecule. While each protein requires an mRNA blueprint, many copies of the protein can
 313 be synthesized from a single mRNA. Factors such as strength of the ribosomal binding site, mRNA
 314 stability, and rare codon usage frequency dictate the number of proteins that can be made from a
 315 single mRNA, with yields ranging from 10^1 to 10^4 (BNID: 104186; 100196; 106254, (34)). Computing
 316 the geometric mean of this range yields ≈ 1000 proteins synthesized per mRNA, a value that agrees
 317 with experimental measurements of the number of proteins per cell ($\approx 3 \times 10^6$, BNID: 100088, (34))
 318 and total number of mRNA per cell ($\approx 3 \times 10^3$, BNID: 100064, (34)).

319 This estimation captures the *steady-state* mRNA copy number, meaning that at any given time,
 320 there will exist approximately 3000 unique mRNA molecules. To determine the *total* number of
 321 mRNA that need to be synthesized over the cell's lifetime, we must consider degradation of the
 322 mRNA. In most bacteria, mRNAs are rather unstable with life times on the order of several minutes
 323 (BNID: 104324; 106253; 111927; 111998, (34)). For convenience, we assume that the typical mRNA
 324 in our cell of interest has a typical lifetime of ≈ 300 seconds. Using this value, we can determine
 325 the total mRNA production rate to maintain a steady-state copy number of 3000 mRNA per cell.
 326 While we direct the reader to the appendix for a more detailed discussion of mRNA transcriptional
 327 dynamics, we state here that the total mRNA production rate must be on the order of ≈ 15 mRNA
 328 per second. In *E. coli*, the average protein is ≈ 300 amino acids in length (BNID: 108986; (34)),
 329 meaning that the corresponding mRNA is ≈ 900 nucleotides which we will further approximate as \approx
 330 1000 nucleotides to account for the non-protein coding regions on the 5' and 3' ends. This means
 331 that the cell must have enough RNA polymerase molecules about to sustain a transcription rate of
 332 $\approx 1.5 \times 10^4$ nucleotides per second. Knowing that a single RNA polymerase polymerizes RNA at a
 333 clip of 40 nucleotides per second, we arrive at a comfortable estimate of ≈ 250 RNA polymerase
 334 complexes needed to satisfy the mRNA demands of the cell. It is worth noting that this number is

335 approximately half of that required to synthesize enough rRNA, as we saw in the previous section.
 336 We find this to be a striking result as these 250 RNA polymerase molecules are responsible for the
 337 transcription of the ≈ 4000 protein coding genes that are not ribosome associated.

338 tRNA

339 The final class of RNA molecules worthy of quantitative consideration is the the pool of tRNAs used
 340 during translation to map codon sequence to amino acid identity. Unlike mRNA or rRNA, each
 341 individual tRNA is remarkably short, ranging from 70 to 95 nucleotides each (BNID: 109645; 102340,
 342 (34)). What they lack in length, they make up for in abundance. There are approximately ≈ 3000
 343 tRNA molecules present for each of the 20 amino acids (BNID: 105280, (34)), although the precise
 344 copy number is dependent on the identity of the ligated amino acid. Using these values, we make
 345 the estimate that $\approx 5 \times 10^6$ nucleotides are sequestered in tRNA per cell. Unlike mRNA, tRNA is
 346 remarkably stable with typical lifetimes *in vivo* on the order of ≈ 48 hours (2; 57) – well beyond the
 347 timescale of division. Once again using our rule-of-thumb for the rate of transcription to be 40
 348 nucleotides per second and assuming a division time of ≈ 5000 seconds, we arrive at an estimate
 349 of ≈ 20 RNA polymerases to synthesize enough tRNA. This requirement pales in comparison to the
 350 number of polymerases needed to generate the rRNA and mRNA pools and can be neglected as a
 351 significant transcriptional burden.

352 RNA Polymerase and σ -factor Abundance

353 These estimates, summarized in **Figure 5** (A), reveal that synthesis of rRNA and mRNA are the
 354 dominant RNA species synthesized by RNA polymerase, suggesting the need for ≈ 700 RNA poly-
 355 merases per cell. As is revealed in **Figure 5** (B), this estimate is about an order of magnitude below
 356 the observed number of RNA polymerase complexes per cell (≈ 5000 - 7000). The disagreement
 357 between the estimated number of RNA polymerases and these observations are at least consistent
 358 with recent literature revealing that ≈ 80 % of RNA polymerases in *E. coli* are not transcriptionally
 359 active (39). Our estimate ignores the possibility that some fraction is only nonspecifically bound to
 360 DNA, as well as the obstacles that RNA polymerase and DNA polymerase present for each other as
 361 they move along the DNA (18).

362 In addition, it is also vital to consider the role of σ -factors which help RNA polymerase identify and
 363 bind to transcriptional start sites (12). Here we consider σ^{70} (RpoD) which is the dominant "general-
 364 purpose" σ -factor in *E. coli*. While initially thought of as being solely involved in transcriptional
 365 initiation, the past two decades of single-molecule work has revealed a more multipurpose role for
 366 σ^{70} including facilitating transcriptional elongation (29; 21; 41; 37; 36). **Figure 5** (B) is suggestive of
 367 such a role as the number of σ^{70} proteins per cell is in close agreement with our estimate of the
 368 number of transcriptional complexes needed.

369 While these estimates and comparison with experimental data reveal an interesting dynamic at
 370 play between the transcriptional demand and copy numbers of the corresponding machinery, these
 371 findings illustrate that transcription cannot be the rate limiting step in bacterial division. **Figure 5**
 372 (A) reveals that the availability of RNA polymerase is not a limiting factor for cell division as the cell
 373 always has an apparent ~ 10 -fold excess than needed. Furthermore, if more transcriptional activity
 374 was needed to satisfy the cellular requirements, more σ^{70} -factors could be expressed to utilize a
 375 larger fraction of the RNA polymerase pool.

376 Protein synthesis

377 Lastly, we turn our attention to the process of translation. So far our estimates have led to protein
 378 copy numbers that are consistent with the proteomic data, or even in excess of what might be
 379 needed for each task under limiting growth conditions. Even in our example of *E. coli* grown under
 380 different carbohydrate sources (**Figure 2(B)**), cells can utilize alternative carbon sources by inducing
 381 the expression of additional membrane transporters and enzymes. Optimal resource allocation
 382 and the role of ribosomal proteins have been an area of intense quantitative study over the last

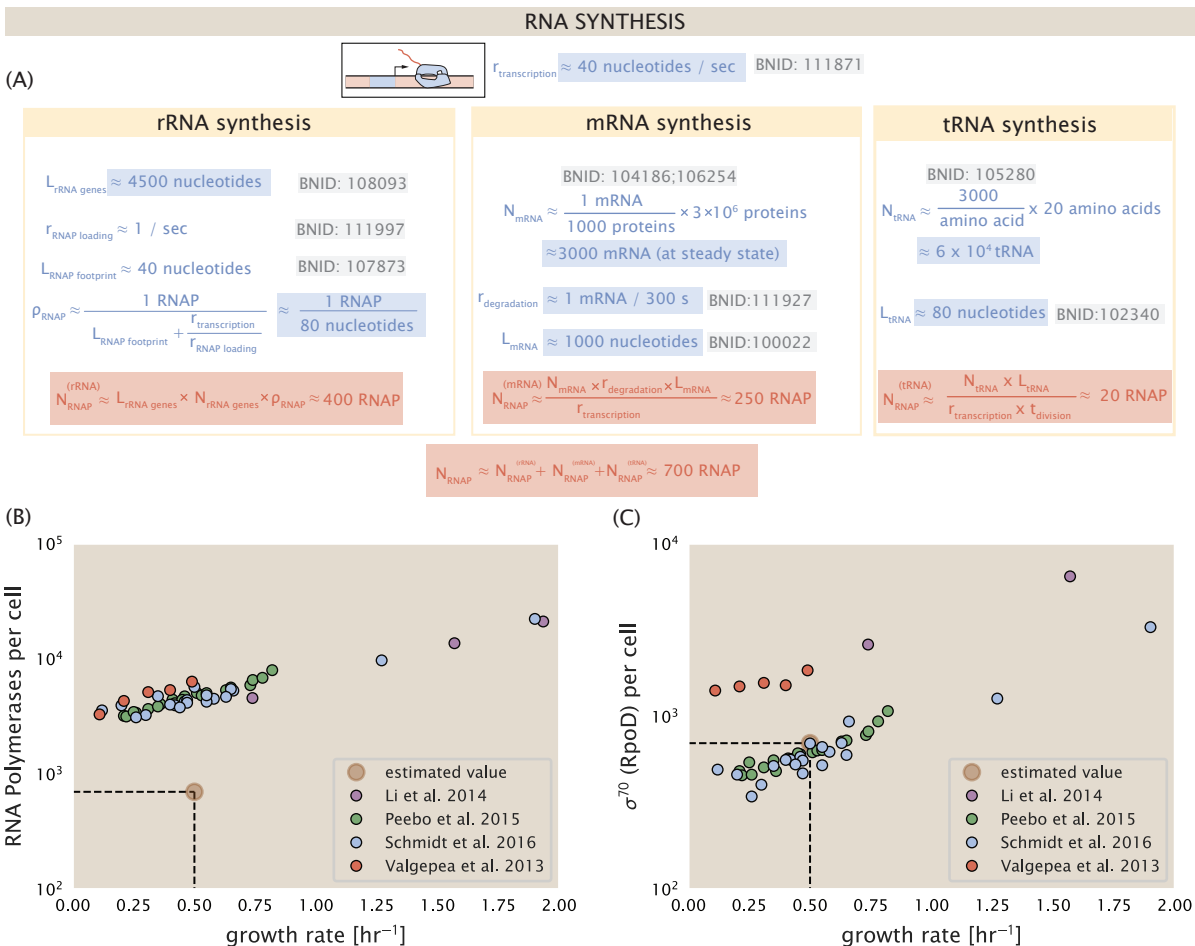


Figure 5. Estimation of the RNA polymerase demand and comparison with experimental data. (A) Estimations for the number of RNA polymerase needed to synthesize sufficient quantities of rRNA, mRNA, and tRNA from left to right, respectively. Bionumber Identifiers (BNIDs) are provided for key quantities used in the estimates. (B) The RNA polymerase core enzyme copy number as a function of growth rate. Colored points correspond to the average number RNA polymerase core enzymes that could be formed given a subunit stoichiometry of $[RpoA]_2[RpoC][RpoB]$. (C) The abundance of σ^{70} as a function of growth rate. Estimated value for the number of RNAP is shown in (B) and (C) as a translucent brown point at a growth rate of 0.5 hr^{-1} .

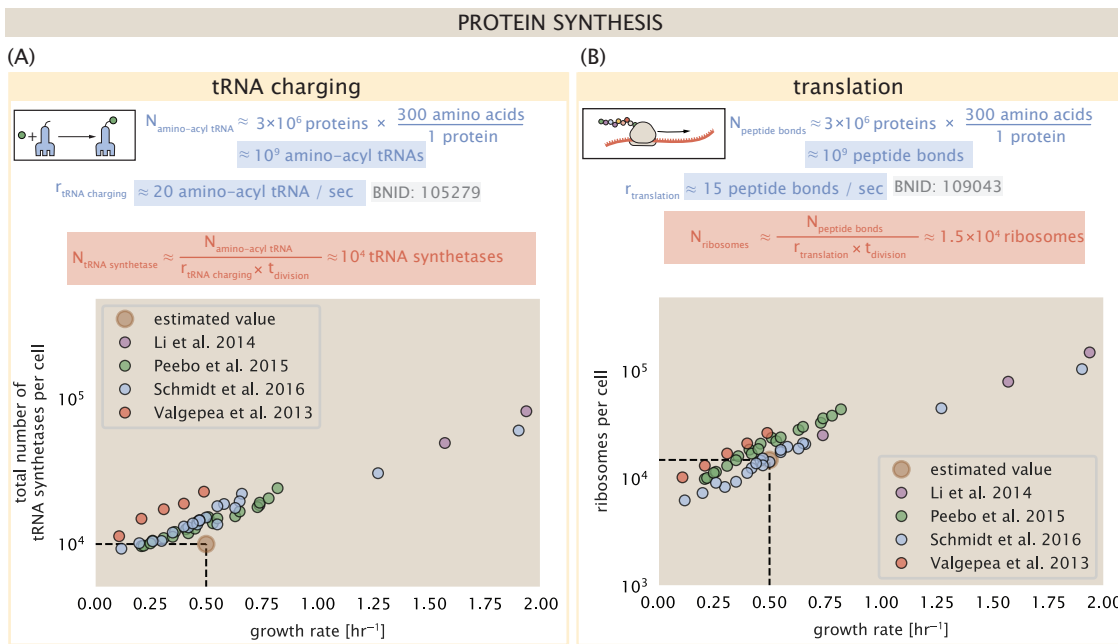


Figure 6. Estimation of the required tRNA synthetases and ribosomes. (A) Estimation for the number of tRNA synthetases that will supply the required amino acid demand. The sum of all tRNA synthetases copy numbers are plotted as a function of growth rate ($[{\text{ArgS}}, {\text{CysS}}, {\text{GlnS}}, {\text{GlxS}}, {\text{IleS}}, {\text{LeuS}}, {\text{ValS}}, {\text{AlaS}}_2, {\text{AsnS}}_2, {\text{AspS}}_2, {\text{TyrS}}_2, {\text{TrpS}}_2, {\text{ThrS}}_2, {\text{SerS}}_2, {\text{ProS}}_2, {\text{PheS}}_2{\text{PheT}}_2, {\text{MetG}}_2, {\text{lysS}}_2, {\text{HisS}}_2, {\text{GlyS}}_2{\text{GlyQ}}_2]$). (B) Estimation for the number of ribosomes required to synthesize all proteins in the cell. The average abundance of ribosomes is plotted as a function of growth rate. Our estimated values are shown for a growth rate of 0.5 hr^{-1} .

383 decade by Hwa and others (50; 24). From the perspective of limiting growth, our earlier estimate
 384 of rRNA highlighted the necessity for multiple copies of rRNA genes in order to make enough
 385 rRNA, suggesting the possibility that synthesis of ribosomes might be rate limiting. While the
 386 transcriptional demand for the ribosomal proteins is substantially lower than rRNA genes, since
 387 many proteins can be translated from relatively fewer mRNA, other ribosomal proteins like the
 388 translation elongation factor EF-Tu also present a substantial burden. For EF-Tu in particular, it is
 389 the most highly expressed protein in *E. coli* and is expressed by multiple genes on the chromosome,
 390 *tufA* and *tufB*.

391 We begin by first estimating the number of tRNA synthetases and ribosomes required for a
 392 doubling time of 5000 seconds. *E. coli* has roughly 3×10^6 proteins per cell, which for an average
 393 protein of 300 aa, amounts to the formation of $\approx 10^9$ peptide bonds. This also corresponds to
 394 the number of amino-acyl tRNA that are used by ribosomes, with the pool of tRNA continuously
 395 recharging new amino acids by tRNA synthetases. At a rate of charging of about 20 amino-acyl tRNA
 396 per second (BNID: 105279, (34)), we find that cells have more than sufficient tRNA synthetases to
 397 meet the demand of ribosomes during protein synthesis (Figure 6(A)). If we consider an elongation
 398 rate of ≈ 15 peptide bonds per second (BNID: 114271, (34; 13)), the formation of $\approx 10^9$ peptide
 399 bonds would require 1.5×10^4 ribosomes at a growth rate of 0.5 hr^{-1} . This is indeed consistent with
 400 the experimental data shown in Figure 6(B).

401 [NB: How about moving this estimates paragraph and associated Figure 6 to SI after all?]

402 We can begin to gain some intuition into how translation might limit growth by noting that the
 403 total number of peptide bonds generated as the cell doubles, N_{aa} , which we used in our calculation
 404 above, will be given by, $\tau \cdot r_t \cdot R$. Here, τ refers to the doubling time of the cell under steady-state
 405 growth, r_t is the maximum translation elongation rate, and R is the average number of ribosomes
 406 per cell. With the growth rate related to the cell doubling time by $\lambda = \ln(2)/\tau$, we can write the

407 translation-limited growth rate as,

$$\lambda_{\text{translation-limited}} = \frac{\ln(2) \cdot r_t \cdot R}{N_{aa}}. \quad (1)$$

408 Alternatively, since N_{aa} is related to the total protein mass through the molecular weight of each
 409 protein, we can also consider the growth rate in terms of ribosomal mass fraction. By making the
 410 approximation that an average amino acid has a molecular weight of 110 Da (see **Figure 7(A)**), we
 411 can rewrite the growth rate as,

$$\lambda_{\text{translation-limited}} \approx \frac{\ln(2) \cdot r_t}{L_R} \Phi_R, \quad (2)$$

412 where L_R is the total length in amino acids that make up a ribosome, and Φ_R is the ribosomal
 413 mass fraction. This is plotted as a function of ribosomal fraction Φ_R in **Figure 7(A)**, where we take
 414 $L_R \approx 7459$ aa, corresponding to the length in amino acids for all ribosomal subunits of the 50S and
 415 30S complex. This formulation assumes that the cell can transcribe the required amount of rRNA,
 416 which appears reasonable for *E. coli* under the allowing us to consider the inherent limit on growth
 417 set by the ribosome.

418 The growth rate defined by Equation 2 reflects mass-balance under steady-state growth and
 419 has long provided a rationalization to the apparent linear increase in *E. coli*'s ribosomal content as
 420 a function of growth rate (Gol; 50). For our purposes, there are several important consequences
 421 of this trend. Perhaps the first thing to notice is that there is a maximum growth rate at about
 422 $\lambda \approx 6\text{hr}^{-1}$, or doubling time of about 7 minutes (dashed line). This growth rate can be viewed as an
 423 inherent maximum growth rate due to the need for the cell to double the cell's entire ribosomal
 424 mass. Interestingly, this limit is independent of the absolute number of ribosomes, but rather
 425 is simply given by time to translate an entire ribosome, L_R/r_t . As shown in **Figure 7(B)**, we can
 426 reconcile this with the observation that in order to double the average number of ribosomes, each
 427 ribosome must produce a second ribosome. This is a process that cannot be parallelized.

428 For reasonable values of Φ_R , between about 0.1 - 0.3 (50), the maximum growth rate is in line
 429 with experimentally reported growth rates around 0.5 - 2 hr^{-1} . Here we are implicitly assuming
 430 that translation proceeds randomly, without preference between ribosomal or non-ribosomal
 431 mRNA, which appears reasonable. Importantly, in order for a cell to scale this growth limit set by
 432 Φ_R , cells *must* increase their ribosomal abundance. This can be achieved by either synthesizing
 433 more ribosomes or reducing the fraction of non-ribosomal proteins. Reduction of non-ribosomal
 434 proteins is not straight forward since, as we have found throughout our estimates, doubling a
 435 cell requires a substantial number of other enzymes and transporters. Increasing the absolute
 436 ribosomal abundance is constrained by production of rRNA.

437 While it is common for bacteria to decrease their ribosomal abundance in poorer nutrient
 438 conditions (50; 32), this does not decrease to zero. From the perspective of a bacterium dealing with
 439 uncertain nutrient conditions, there is likely a benefit for the cell to maintain some relative fraction
 440 of ribosomes to support rapid growth as nutrient conditions improve. However, if we consider
 441 a scenario where nutrient conditions become poorer and poorer, there will be a regime where
 442 ribosomes are in excess of the nutrient supply. If the cell is to maintain steady-state growth, it will
 443 need to attenuate its translational activity since ribosomes would otherwise exhaust their supply of
 444 amino acids and bring cell growth to a halt (**Figure 7(C)**). In the next section we will consider this
 445 more specifically for *E. coli*, which has been shown to maintain a relatively high elongation rate even
 446 in stationary phase (≈ 8 aa/s, (13)) where cell growth is minimal.

447 [NB: I'm considering moving this paragraph near the end of the next section].

448 **Multiple replication forks bias ribosome abundance.**

449 *E. coli* cells grow by an adder mechanism, whereby cells add a constant volume with each cell
 450 division (59). In conjunction with this, additional rounds of DNA replication are triggered when cells
 451 reach a critical volume per origin of replication (**Figure 8(A)**). This leads to the classically-described

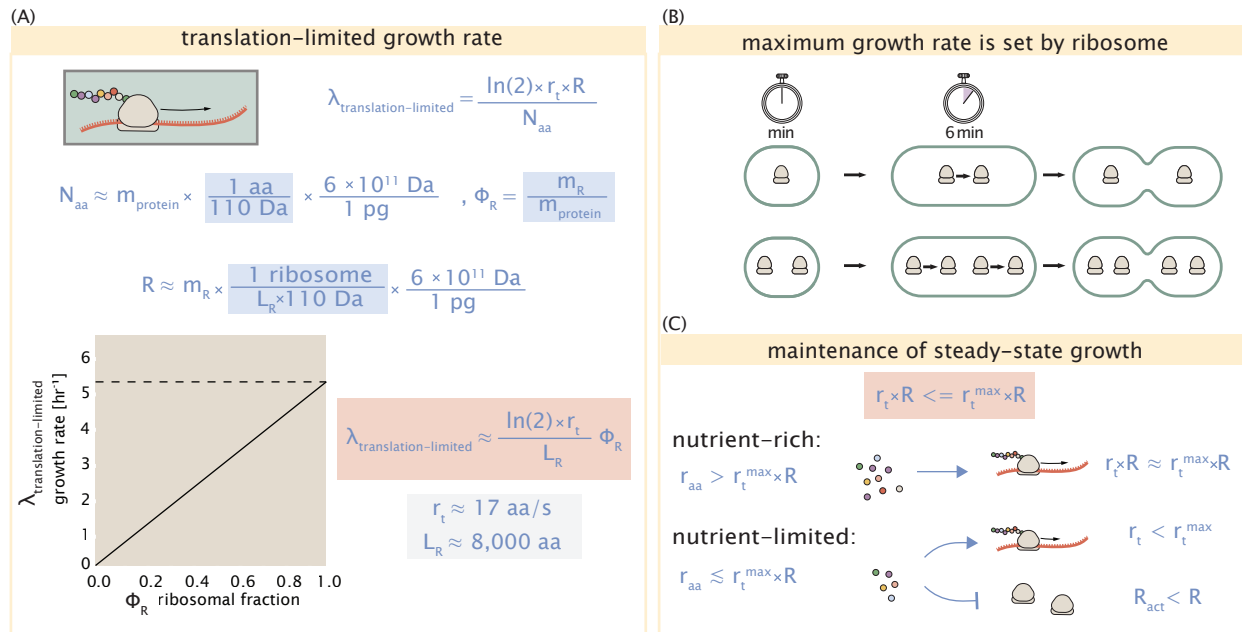


Figure 7. Translation-limited growth rate. (A) Here we consider the translation-limited growth as a function of ribosomal fraction. By mass balance, the time required to double the entire proteome (N_{aa} / r_t) sets the translation-limited growth rate, $\lambda_{\text{translation-limited}}$. Here N_{aa} is effectively the number of peptide bonds that must be translated, r_t is the translation elongation rate, and R is the number of ribosomes. This can also be re-written in terms of the ribosomal mass fraction $\Phi_R = m_R / m_{\text{protein}}$, where m_R is the total ribosomal mass and m_{protein} is the mass of all proteins in the cell. L_R refers to the summed length of the ribosome in amino acids. $\lambda_{\text{translation-limited}}$ is plotted as a function of Φ_R (solid line). (B) The dashed line in part (A) identifies a maximum growth rate that is set by the ribosome. Specifically, this growth rate corresponds to the time required to translate an entire ribosome, L_R / r_t . This is a result that is independent of the number of ribosomes in the cell as shown schematically here. (C) Schematic showing translation-specific requirements for maintenance of steady-state growth. In a nutrient rich environment, amino acid supply r_{aa} is sufficiently in excess of demand by ribosomes translating at their maximal rate. In poorer nutrient conditions, reduced amino acid supply r_{aa} will decrease the rate of elongation. In a regime where r_{aa} is less than $r_t \cdot R$, the number of actively translating ribosomes will need to be reduced in order to maintain steady-state growth.

452 exponential increase in cell size with growth rate (47; 53; 52). In the context of maximizing growth
 453 rate, it is notable that the majority of ribosomal proteins and rRNA operons are found closer to the
 454 DNA origin. Given the need to increase total gene dosage of rRNA operons at faster growth rates,
 455 this raises the possibility that the observed size scaling and increase in chromosomal equivalents
 456 might simply be a means for the cell to tune biosynthesis according to their physiological state.

457 While an increase in transcription has been observed for genes near the origin in rapidly growing
 458 *E. coli* (49), we were unaware of such characterization at the proteomic level. In order to test whether
 459 there is a relative increase in protein expression for genes closer to the origin, we calculated a
 460 running boxcar average of protein copy number as a function of each gene's transcriptional start site.
 461 While absolute protein copy numbers can vary substantially across the chromosome, we indeed
 462 observe a bias in expression under fast growth conditions (**Figure 8(B)**, showing the result using
 463 a 0.5 kb averaging window). The dramatic change in protein copy number near the origin mainly
 464 reflects the increase in ribosomal protein expression. This trend is in contrast to slower growth
 465 conditions where the average copy number is more uniform across the length of the chromosome.

466 If ribosomal genes (rRNA and ribosomal proteins) are being synthesized according to their
 467 available gene dosage we can make two related hypotheses about how their abundance should
 468 vary with chromosomal content. The first is that the ribosomal protein fraction should increase
 469 in proportion to the average ratio of DNA origins to DNA termini ($\langle \# \text{ ori} \rangle / \langle \# \text{ ter} \rangle$ ratio). This is
 470 a consequence of the skew in DNA dosage as cells grow faster. The second is that the absolute
 471 number of ribosomes should increase in proportion to the number of DNA origins ($\langle \# \text{ ori} \rangle$), since
 472 this will reflect the total gene dosage at a particular growth condition.

473 In order to test each of these expectations we considered the experimental data from Si *et al.* (2017), which inferred these parameters for cells under nutrient-limited growth. $\langle \# \text{ ori} \rangle / \langle \# \text{ ter} \rangle$ ratio depends on how quickly chromosomes are replicated relative the cell's doubling time
 474 τ and is given by $2^{\tau_C/\tau}$. Here τ_C is the time taken to replicate *E. coli*'s chromosome, referred to
 475 as the C period of cell division. In **Figure 8(C)** we plot τ_C versus τ that were measured, with data
 476 points in red corresponding to *E. coli* strain MG1655, and blue to strain NCM3722. In their work
 477 they also measured the total RNA to protein ratio which reflects ribosomal abundance and we
 478 show that data along with other recent measurements from Dai *et al.*. Indeed we find that the
 479 ribosomal fraction increases with $\langle \# \text{ ori} \rangle / \langle \# \text{ ter} \rangle$ (**Figure 8(C)**). Across our different proteomic
 480 data sets there also appeared two distinct trends. To consider the possibility that this may reflect
 481 systematic differences in how the data was generated, we also considered recent measurements of
 482 total RNA to protein ratio across the growth rates considered, which provide an alternative measure
 483 of ribosomal abundance (RNA to protein ratio $\approx \Phi_R \times 2.1$ (13)). While these showed a similar
 484 correlation, they were most consistent with the proteomic data from Schmidt *et al.* (2016) and Li *et
 485 al.* (2014).

486 We can similarly estimate $\langle \# \text{ ori} \rangle$, which depends on how often replication forks are initiated
 487 per cell cycle. This is given by the number of overlapping cell cycles, $2^{\tau_{\text{cyc}}/\tau}$, where τ_{cyc} refers to
 488 the total time of chromosome replication and cell division. **Figure 8(E)** shows the associated data
 489 from Si *et al.*, which we use to estimate $\langle \# \text{ ori} \rangle$ for each growth condition of the proteomic data. In
 490 agreement with our expectations, we find a strong correlation between the ribosome copy number
 491 and estimated $\langle \# \text{ ori} \rangle$ (**Figure 8(F)**).

492 [NB: to do. 1) slow growth regime, 2) putting it all together ; cells appear to grow near the
 493 translation-limited rate ($r_i = 17 \text{ aa/s}$) across all growth conditions. Need to provide some rationalization
 494 for points above line.]

495 [NB: to incorporate. Titration of the cellular ppGpp concentration invoked similar proteomic
 496 changes to those observed under nutrient limitation (66). In light of our hypothesis that such
 497 changes to the proteome are intimately linked to the details of DNA replication, it was recently
 498 shown that both the $\langle \# \text{ ori} \rangle / \langle \# \text{ ter} \rangle$ and cell size lost their growth rate dependent scaling in a
 499 ppGpp null strain. Rather, cells exhibit a $\langle \# \text{ ori} \rangle / \langle \# \text{ ter} \rangle$ closer to 4 and cell size more consistent
 500 with a fast growth state (16). This supports the possibility that in addition to coordinating ribosome
 501

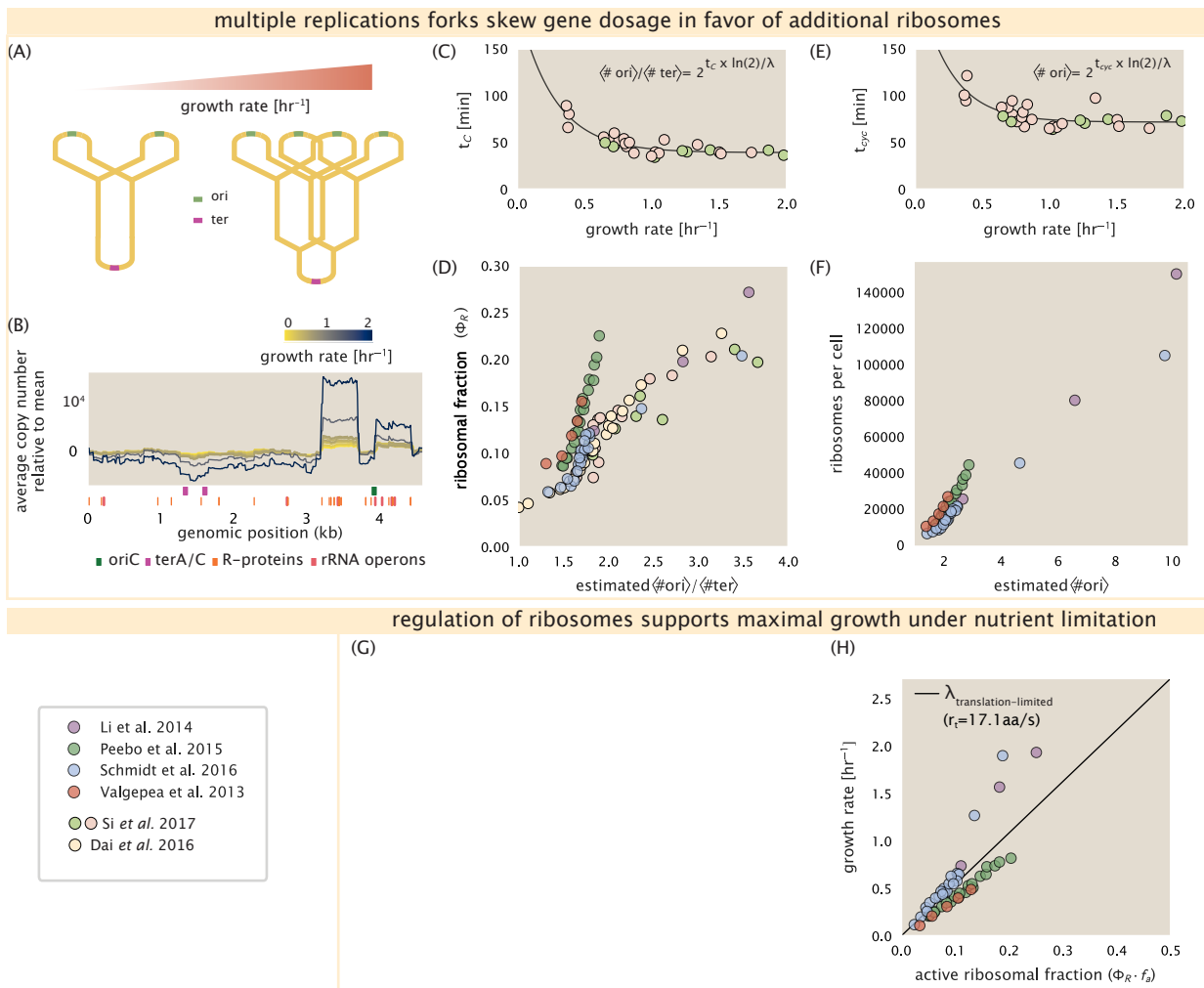


Figure 8. Multiple replication forks skew gene dosage and ribosomal content. (A) Schematic shows the expected increase in replication forks (or number of ori regions) as *E. coli* cells grow faster. (B) A running boxcar average of protein copy number is calculated for each growth condition considered by Schmidt *et al.*. A 0.5 kb averaging window was used. Protein copy numbers are reported relative to their condition-specific means in order to center all data sets. (C) and (E) show experimental data from Si *et al.* (2017). Solid lines show fits to the data, which were used to estimate $\langle \# \text{ori} \rangle / \langle \# \text{ter} \rangle$ [NB: to note fit equations]. Red data points correspond to measurements in strain MG1655, while light green points are for strain NCM3722. (D) Plot compares our estimate of $\langle \# \text{ori} \rangle / \langle \# \text{ter} \rangle$ to the experimental measurements of ribosomal abundance. Ribosomal fraction was approximated from the RNA/protein ratios of Dai *et al.* (2016) (yellow) and Si *et al.* (2017) (light red and light green) by the conversion RNA/protein ratio $\approx \Phi_R \cdot 2.1$. (F) plots the ribosome copy number estimated from the proteomic data against our estimate of $\langle \# \text{ori} \rangle$. (G) [in progress], (H) Experimental data from Dai *et al.* are used to estimate the fraction of actively translating ribosomes. The solid line represents the translation-limited growth rate for ribosomes elongating at 17.1 aa/s.

503 activity, (p)ppGpp signaling may be acting to coordinate other cellular processes in accordance with
 504 nutrient conditions and biosynthetic demand. From this perspective, the increase in the rate of
 505 DNA initiation and associated increase in cell size may be viewed as a way for the cell to vary its
 506 proteomic composition and biosynthetic capacity according to its available nutrient conditions.]

507 References

- 508 [Gol] *Regulation of the Protein-Synthesizing Machinery—Ribosomes, tRNA, Factors, and So On.*
- 509 [2] Abelson, H., Johnson, L., Penman, S., and Green, H. (1974). Changes in RNA in relation to growth of the
 510 fibroblast: II. The lifetime of mRNA, rRNA, and tRNA in resting and growing cells. *Cell*, 1(4):161–165.
- 511 [3] Aidelberg, G., Towbin, B. D., Rothschild, D., Dekel, E., Bren, A., and Alon, U. (2014). Hierarchy of non-glucose
 512 sugars in Escherichia coli. *BMC Systems Biology*, 8(1):133.
- 513 [4] Antonenko, Y. N., Pohl, P., and Denisov, G. A. (1997). Permeation of ammonia across bilayer lipid membranes
 514 studied by ammonium ion selective microelectrodes. *Biophysical Journal*, 72(5):2187–2195.
- 515 [5] Ason, B., Bertram, J. G., Hingorani, M. M., Beechem, J. M., O'Donnell, M., Goodman, M. F., and Bloom, L. B.
 516 (2000). A Model for *Escherichia coli* DNA Polymerase III Holoenzyme Assembly at Primer/Template Ends:
 517 DNA Triggers A Change In Binding Specificity of the γ Complex Clamp Loader. *Journal of Biological Chemistry*,
 518 275(4):3006–3015.
- 519 [6] Assentoft, M., Kaptan, S., Schneider, H.-P., Deitmer, J. W., de Groot, B. L., and MacAulay, N. (2016). Aquaporin
 520 4 as a NH₃ Channel. *Journal of Biological Chemistry*, 291(36):19184–19195.
- 521 [7] Bauer, S. and Ziv, E. (1976). Dense growth of aerobic bacteria in a bench-scale fermentor. *Biotechnology and
 522 Bioengineering*, 18(1):81–94. _eprint: <https://onlinelibrary.wiley.com/doi/10.1002/bit.260180107>.
- 523 [8] Belliveau, N. M., Barnes, S. L., Ireland, W. T., Jones, D. L., Sweredoski, M. J., Moradian, A., Hess, S., Kinney,
 524 J. B., and Phillips, R. (2018). Systematic approach for dissecting the molecular mechanisms of transcriptional
 525 regulation in bacteria. *Proceedings of the National Academy of Sciences*, 115(21):E4796–E4805.
- 526 [9] Birnbaum, L. S. and Kaplan, S. (1971). Localization of a Portion of the Ribosomal RNA Genes in *Escherichia
 527 coli*. *Proceedings of the National Academy of Sciences*, 68(5):925–929.
- 528 [10] Booth, I. R., Mitchell, W. J., and Hamilton, W. A. (1979). Quantitative analysis of proton-linked transport
 529 systems. The lactose permease of *Escherichia coli*. *Biochemical Journal*, 182(3):687–696.
- 530 [11] Bremer, H. and Dennis, P. P. (2008). Modulation of Chemical Composition and Other Parameters of the Cell
 531 at Different Exponential Growth Rates. *EcoSal Plus*, 3(1).
- 532 [12] Browning, D. F. and Busby, S. J. W. (2016). Local and global regulation of transcription initiation in bacteria.
 533 *Nature Reviews Microbiology*, 14(10):638–650.
- 534 [13] Dai, X., Zhu, M., Warren, M., Balakrishnan, R., Patsalo, V., Okano, H., Williamson, J. R., Fredrick, K., Wang,
 535 Y.-P., and Hwa, T. (2016). Reduction of translating ribosomes enables *Escherichia coli* to maintain elongation
 536 rates during slow growth. *Nature Microbiology*, 2(2):16231.
- 537 [14] Escalante, A., Salinas Cervantes, A., Gosset, G., and Bolívar, F. (2012). Current knowledge of the *Escherichia
 538 coli* phosphoenolpyruvate–carbohydrate phosphotransferase system: Peculiarities of regulation and impact
 539 on growth and product formation. *Applied Microbiology and Biotechnology*, 94(6):1483–1494.
- 540 [15] Feist, A. M., Henry, C. S., Reed, J. L., Krummenacker, M., Joyce, A. R., Karp, P. D., Broadbelt, L. J., Hatzimanikatis,
 541 V., and Palsson, B. Ø. (2007). A genome-scale metabolic reconstruction for *Escherichia coli* K-12 MG1655 that
 542 accounts for 1260 ORFs and thermodynamic information. *Molecular Systems Biology*, 3(1):121.
- 543 [16] Fernández-Coll, L., Maciąg-Dorszynska, M., Tailor, K., Vadia, S., Levin, P. A., Szalewska-Palasz, A., Cashel, M.,
 544 and Dunny, G. M. (2020). The Absence of (p)ppGpp Renders Initiation of *Escherichia coli* Chromosomal DNA
 545 Synthesis Independent of Growth Rates. *mBio*, 11(2):45.
- 546 [17] Fijalkowska, I. J., Schaaper, R. M., and Jonczyk, P. (2012). DNA replication fidelity in *Escherichia coli*: A
 547 multi-DNA polymerase affair. *FEMS Microbiology Reviews*, 36(6):1105–1121.
- 548 [18] Finkelstein, I. J. and Greene, E. C. (2013). Molecular Traffic Jams on DNA. *Annual Review of Biophysics*,
 549 42(1):241–263.

- 550 [19] Gama-Castro, S., Salgado, H., Santos-Zavaleta, A., Ledezma-Tejeida, D., Muñiz-Rascado, L., García-Sotelo,
 551 J. S., Alquicira-Hernández, K., Martínez-Flores, I., Pannier, L., Castro-Mondragón, J. A., Medina-Rivera, A., Solano-
 552 Lira, H., Bonavides-Martínez, C., Pérez-Rueda, E., Alquicira-Hernández, S., Porrón-Sotelo, L., López-Fuentes,
 553 A., Hernández-Koutoucheva, A., Moral-Chávez, V. D., Rinaldi, F., and Collado-Vides, J. (2016). RegulonDB
 554 version 9.0: High-level integration of gene regulation, coexpression, motif clustering and beyond. *Nucleic
 555 Acids Research*, 44(D1):D133–D143.
- 556 [20] Ge, J., Yu, G., Ator, M. A., and Stubbe, J. (2003). Pre-Steady-State and Steady-State Kinetic Analysis of *E. coli*
 557 Class I Ribonucleotide Reductase. *Biochemistry*, 42(34):10071–10083.
- 558 [21] Goldman, S. R., Nair, N. U., Wells, C. D., Nickels, B. E., and Hochschild, A. (2015). The primary σ factor in
 559 *Escherichia coli* can access the transcription elongation complex from solution *in vivo*. *eLife*, 4:e10514.
- 560 [22] Harris, R. M., Webb, D. C., Howitt, S. M., and Cox, G. B. (2001). Characterization of PitA and PitB from
 561 *Escherichia coli*. *Journal of Bacteriology*, 183(17):5008–5014.
- 562 [23] Heldal, M., Norland, S., and Tumyr, O. (1985). X-ray microanalytic method for measurement of dry matter
 563 and elemental content of individual bacteria. *Applied and Environmental Microbiology*, 50(5):1251–1257.
- 564 [24] Hui, S., Silverman, J. M., Chen, S. S., Erickson, D. W., Basan, M., Wang, J., Hwa, T., and Williamson, J. R. (2015).
 565 Quantitative proteomic analysis reveals a simple strategy of global resource allocation in bacteria. *Molecular
 566 Systems Biology*, 11(2):e784–e784.
- 567 [25] Ireland, W. T., Beeler, S. M., Flores-Bautista, E., Belliveau, N. M., Sweredoski, M. J., Moradian, A., Kinney, J. B.,
 568 and Phillips, R. (2020). Deciphering the regulatory genome of *Escherichia coli*, one hundred promoters at a
 569 time. *bioRxiv*.
- 570 [26] Jacob, F. and Monod, J. (1961). Genetic regulatory mechanisms in the synthesis of proteins. *Journal of
 571 Molecular Biology*, 3(3):318–356.
- 572 [27] Jensen, R. B., Wang, S. C., and Shapiro, L. (2001). A moving DNA replication factory in Caulobacter crescentus.
 573 *The EMBO journal*, 20(17):4952–4963.
- 574 [28] Jun, S., Si, F., Pugatch, R., and Scott, M. (2018). Fundamental principles in bacterial physiology - history,
 575 recent progress, and the future with focus on cell size control: A review. *Reports on Progress in Physics*,
 576 81(5):056601.
- 577 [29] Kapanidis, A. N., Margeat, E., Laurence, T. A., Doose, S., Ho, S. O., Mukhopadhyay, J., Kortkhonja, E., Mekler,
 578 V., Ebright, R. H., and Weiss, S. (2005). Retention of Transcription Initiation Factor Σ 70 in Transcription
 579 Elongation: Single-Molecule Analysis. *Molecular Cell*, 20(3):347–356.
- 580 [30] Khademi, S., O'Connell, J., Remis, J., Robles-Colmenares, Y., Miercke, L. J. W., and Stroud, R. M. (2004).
 581 Mechanism of Ammonia Transport by Amt/MEP/Rh: Structure of AmtB at 1.35 Å. *Science*, 305(5690):1587–
 582 1594.
- 583 [31] Li, G.-W., Burkhardt, D., Gross, C., and Weissman, J. S. (2014). Quantifying absolute protein synthesis rates
 584 reveals principles underlying allocation of cellular resources. *Cell*, 157(3):624–635.
- 585 [32] Liebermeister, W., Noor, E., Flamholz, A., Davidi, D., Bernhardt, J., and Milo, R. (2014). Visual account of
 586 protein investment in cellular functions. *Proceedings of the National Academy of Sciences*, 111(23):8488–8493.
- 587 [33] Liu, M., Durfee, T., Cabrera, J. E., Zhao, K., Jin, D. J., and Blattner, F. R. (2005). Global Transcriptional Programs
 588 Reveal a Carbon Source Foraging Strategy by *Escherichia coli*. *Journal of Biological Chemistry*, 280(16):15921–
 589 15927.
- 590 [34] Milo, R., Jorgensen, P., Moran, U., Weber, G., and Springer, M. (2010). BioNumbers—the database of key
 591 numbers in molecular and cell biology. *Nucleic Acids Research*, 38(suppl_1):D750–D753.
- 592 [35] Monod, J. (1947). The phenomenon of enzymatic adaptation and its bearings on problems of genetics and
 593 cellular differentiation. *Growth Symposium*, 9:223–289.
- 594 [36] Mooney, R. A., Darst, S. A., and Landick, R. (2005). Sigma and RNA Polymerase: An On-Again, Off-Again
 595 Relationship? *Molecular Cell*, 20(3):335–345.
- 596 [37] Mooney, R. A. and Landick, R. (2003). Tethering Σ 70 to RNA polymerase reveals high *in vivo* activity of σ
 597 factors and Σ 70-dependent pausing at promoter-distal locations. *Genes & Development*, 17(22):2839–2851.

- 598 [38] Neidhardt, F. C., Ingraham, J., and Schaechter, M. (1991). *Physiology of the Bacterial Cell - A Molecular Approach*, volume 1. Elsevier.
- 600 [39] Patrick, M., Dennis, P. P., Ehrenberg, M., and Bremer, H. (2015). Free RNA polymerase in *Escherichia coli*. *Biochimie*, 119:80–91.
- 602 [40] Peebo, K., Valgepea, K., Maser, A., Nahku, R., Adamberg, K., and Vilu, R. (2015). Proteome reallocation in
603 *Escherichia coli* with increasing specific growth rate. *Molecular BioSystems*, 11(4):1184–1193.
- 604 [41] Perdue, S. A. and Roberts, J. W. (2011). σ^{70} -dependent Transcription Pausing in *Escherichia coli*. *Journal of Molecular Biology*, 412(5):782–792.
- 606 [42] Phillips, R. (2018). Membranes by the Numbers. In *Physics of Biological Membranes*, pages 73–105. Springer,
607 Cham, Cham.
- 608 [43] Ramos, S. and Kaback, H. R. (1977). The relation between the electrochemical proton gradient and active
609 transport in *Escherichia coli* membrane vesicles. *Biochemistry*, 16(5):854–859.
- 610 [44] Rosenberg, H., Gerdes, R. G., and Chegwidden, K. (1977). Two systems for the uptake of phosphate in
611 *Escherichia coli*. *Journal of Bacteriology*, 131(2):505–511.
- 612 [45] Rudd, S. G., Valerie, N. C. K., and Helleday, T. (2016). Pathways controlling dNTP pools to maintain genome
613 stability. *DNA Repair*, 44:193–204.
- 614 [46] Sánchez-Romero, M. A., Molina, F., and Jiménez-Sánchez, A. (2011). Organization of ribonucleoside
615 diphosphate reductase during multifork chromosome replication in *Escherichia coli*. *Microbiology*, 157(8):2220–
616 2225.
- 617 [47] Schaechter, M., Maaløe, O., and Kjeldgaard, N. O. (1958). Dependency on Medium and Temperature
618 of Cell Size and Chemical Composition during Balanced Growth of *Salmonella typhimurium*. *Microbiology*,
619 19(3):592–606.
- 620 [48] Schmidt, A., Kochanowski, K., Vedelaar, S., Ahrné, E., Volkmer, B., Callipo, L., Knoops, K., Bauer, M., Aebersold,
621 R., and Heinemann, M. (2016). The quantitative and condition-dependent *Escherichia coli* proteome. *Nature Biotechnology*, 34(1):104–110.
- 623 [49] Scholz, S. A., Diao, R., Wolfe, M. B., Fivenson, E. M., Lin, X. N., and Freddolino, P. L. (2019). High-Resolution
624 Mapping of the *Escherichia coli* Chromosome Reveals Positions of High and Low Transcription. *Cell Systems*,
625 8(3):212–225.e9.
- 626 [50] Scott, M., Gunderson, C. W., Mateescu, E. M., Zhang, Z., and Hwa, T. (2010). Interdependence of cell growth
627 and gene expression: origins and consequences. *Science*, 330(6007):1099–1102.
- 628 [51] Sekowska, A., Kung, H.-F., and Danchin, A. (2000). Sulfur Metabolism in *Escherichia coli* and Related Bacteria:
629 Facts and Fiction. *Journal of Molecular Microbiology and Biotechnology*, 2(2):34.
- 630 [52] Si, F., Le Treut, G., Sauls, J. T., Vadia, S., Levin, P. A., and Jun, S. (2019). Mechanistic Origin of Cell-Size Control
631 and Homeostasis in Bacteria. *Current Biology*, 29(11):1760–1770.e7.
- 632 [53] Si, F., Li, D., Cox, S. E., Sauls, J. T., Azizi, O., Sou, C., Schwartz, A. B., Erickstad, M. J., Jun, Y., Li, X., and Jun,
633 S. (2017). Invariance of Initiation Mass and Predictability of Cell Size in *Escherichia coli*. *Current Biology*,
634 27(9):1278–1287.
- 635 [54] Sirko, A., Zatyka, M., Sadowy, E., and Hulanicka, D. (1995). Sulfate and thiosulfate transport in *Escherichia coli* K-12: Evidence for a functional overlapping of sulfate- and thiosulfate-binding proteins. *Journal of Bacteriology*, 177(14):4134–4136.
- 638 [55] Stasi, R., Neves, H. I., and Spira, B. (2019). Phosphate uptake by the phosphonate transport system PhnCDE.
639 *BMC Microbiology*, 19.
- 640 [56] Stevenson, B. S. and Schmidt, T. M. (2004). Life History Implications of rRNA Gene Copy Number in
641 *Escherichia coli*. *Applied and Environmental Microbiology*, 70(11):6670–6677.
- 642 [57] Svenningsen, S. L., Kongstad, M., Stenum, T. S. n., Muñoz-Gómez, A. J., and Sørensen, M. A. (2017).
643 Transfer RNA is highly unstable during early amino acid starvation in *Escherichia coli*. *Nucleic Acids Research*,
644 45(2):793–804.

- 645 [58] Szenk, M., Dill, K. A., and de Graff, A. M. R. (2017). Why Do Fast-Growing Bacteria Enter Overflow Metabolism?
646 Testing the Membrane Real Estate Hypothesis. *Cell Systems*, 5(2):95–104.
- 647 [59] Taheri-Araghi, S., Bradde, S., Sauls, J. T., Hill, N. S., Levin, P. A., Paulsson, J., Vergassola, M., and Jun, S. (2015).
648 Cell-size control and homeostasis in bacteria. - PubMed - NCBI. *Current Biology*, 25(3):385–391.
- 649 [60] Taymaz-Nikerel, H., Borujeni, A. E., Verheijen, P. J. T., Heijnen, J. J., and van Gulik, W. M.
650 (2010). Genome-derived minimal metabolic models for *Escherichia coli* MG1655 with estimated
651 in vivo respiratory ATP stoichiometry. *Biotechnology and Bioengineering*, 107(2):369–381. _eprint:
652 <https://onlinelibrary.wiley.com/doi/pdf/10.1002/bit.22802>.
- 653 [61] Valgepea, K., Adamberg, K., Seiman, A., and Vilu, R. (2013). *Escherichia coli* achieves faster growth by
654 increasing catalytic and translation rates of proteins. *Molecular BioSystems*, 9(9):2344.
- 655 [62] van Heeswijk, W. C., Westerhoff, H. V., and Boogerd, F. C. (2013). Nitrogen Assimilation in *Escherichia coli*:
656 Putting Molecular Data into a Systems Perspective. *Microbiology and Molecular Biology Reviews*, 77(4):628–695.
- 657 [63] Willsky, G. R., Bennett, R. L., and Malamy, M. H. (1973). Inorganic Phosphate Transport in *Escherichia coli*:
658 Involvement of Two Genes Which Play a Role in Alkaline Phosphatase Regulation. *Journal of Bacteriology*,
659 113(2):529–539.
- 660 [64] Zhang, L., Jiang, W., Nan, J., Almqvist, J., and Huang, Y. (2014a). The *Escherichia coli* CysZ is a pH dependent
661 sulfate transporter that can be inhibited by sulfite. *Biochimica et Biophysica Acta (BBA) - Biomembranes*,
662 1838(7):1809–1816.
- 663 [65] Zhang, Z., Aboulwafa, M., and Saier, M. H. (2014b). Regulation of crp gene expression by the catabolite
664 repressor/activator, cra, in *Escherichia coli*. *Journal of Molecular Microbiology and Biotechnology*, 24(3):135–141.
- 665 [66] Zhu, M. and Dai, X. (2019). Growth suppression by altered (p)ppGpp levels results from non-optimal
666 resource allocation in *Escherichia coli*. *Nucleic Acids Research*, 47(9):4684–4693.